Journal of The Electrochemical Society, **151** (2) B45-B52 (2004)
0013-4651/2004/151(2)/B45/8/$7.00 © The Electrochemical Society, Inc.

Kinetic Model for Aluminum Dissolution in Corrosion Pits

Kamal Muthukrishnan and Kurt R. Hebert*,z

Department of Chemical Engineering, Iowa State University, Ames, Iowa 50011, USA

The kinetics of aluminum dissolution in etch pits and tunnels, in a 1 M HCl-3 M H_2SO_4 solution at 70°C, were investigated. Dissolution current densities during growth of tunnels and pits, at potentials of roughly −0.8 and 1 V *vs.* Ag/AgCl respectively, were found to be approximately 6 A/cm^2. Transient experiments using current step reductions during pitting, or anodic current pulses during tunnel growth, revealed strongly potential-dependent current densities up to 300 A/cm^2. The results suggested that the dissolution rate is potential-dependent when measured on times scales of ~1 ms after potential disturbances, but insensitive to potential in quasi-stationary experiments. A kinetic model was presented assuming a monolayer or multilayer chloride layer on the aluminum surface, including kinetic expressions for transfer of Al^{+3} and Cl^- ions at the film/solution interface, and ionic conduction in the film. In agreement with experiments, the model yields constant or potential-dependent dissolution rates following a Butler-Volmer relation, depending on the time scale of experimental measurements. The large current densities in anodic transient experiments derived from high rates of Cl^- incorporation during film growth.
 [DOI: 10.1149/1.1635386]

Manuscript submitted March 28, 2003; revised manuscript received August 2, 2003. Available electronically January 9, 2004.

Models of metal dissolution in corrosion pits are important for predictions of pit growth rates and stability, so that eventually environmental conditions for failure can be determined. Prior investigations of aluminum pitting have focused on the nature of processes controlling the metal dissolution rate. Different studies have found that the corrosion rate is determined by solution-phase ohmic conduction,[1,2] mass transport,[3,4] or have found mixed ohmic and transport control.[5-7] The general picture suggested is that the surface kinetic resistance for dissolution is small, and that depending on experimental conditions such as solution composition or potential, transport or conduction may control the rate of the process. However, a kinetic model of dissolution would be useful to predict regimes of control by mass transport, ohmic resistance or kinetics. Such a model would also provide a chemical description of the dissolving surface, which would help elucidate conditions where either dissolution or oxide passivation should occur.

There have been relatively few attempts to obtain a fundamental chemical model of the dissolving aluminum surface during localized corrosion. Some authors have suggested that the surface is covered by a resistive metal chloride film, which absorbs the large overpotential frequently associated with pit growth.[8-10] Beck has carried out studies of aluminum dissolution at high potentials in millimeter-scale artificial pits, which revealed conduction and structural properties of $AlCl_3$ surface films found in these circumstances.[11,12] However, it is not known whether similar films are found in naturally-occurring pits. Experimental kinetic studies of oxide passivation in aluminum pits were carried out by the present authors, and a model for passivation was presented.[13-16] Those investigations found evidence that a pit surface is covered by a monolayer of chloride, at potentials near the critical potential for repassivation; chloride desorption from this layer initiates oxide film growth.

Earlier work by the present authors has explored dissolution kinetics in aluminum etch pits and tunnels, during anodic etching in hot chloride-containing solutions. Tunnels are elongated corrosion cavities which form by passivation of the sidewalls of etch pits while dissolution continues on the pit's bottom face.[17,18] Etch pits predominate at times of the order of 100 ms, while tunnels are most prevalent after several seconds. The number densities of pits and tunnels are comparable in magnitude (10^5 to 10^7 cm^{-2}). The growth current density of etch tunnels was measured using slow modulations of the applied etching current and was found to be constant at a given temperature, and of the order of 10 A/cm^2.[19] Current densities in etch pits, at etch times smaller than 100 ms, were inferred from pit size distributions measured with scanning electron microscopy (SEM), and were found to be consistent with tunnel current densities for the same etching conditions.[20] While tunnels grow at potentials of −0.8-0.9 V *vs.* saturated calomel electrode (SCE), potentials higher than 1 V were present during the pitting experiments. Hence, these measurements suggested that the dissolution current density is insensitive to potential. In another kinetic study of dissolution in tunnels, the potential driving force for dissolution was measured within 0.1 ms after step increases of applied current during etching.[21] Contrary to the earlier measurements of pit growth rates, the results indicated a Tafel-type exponential current/potential relationship, with dissolution current densities as high as 100 A/cm^2.

The present work addresses the issue of the potential dependence of the dissolution current density. Further measurements of the dissolution rate of pits and tunnels are presented, as well as transient measurements of dissolution kinetics using current steps and pulses. Together, the new and previous kinetic measurements show that potential-dependent or potential-insensitive dissolution rates are associated with transient or quasi-stationary experiments, respectively. A new kinetic model for aluminum dissolution is then described which provides for the time scale-dependent kinetics found experimentally. According to the model, the corroding surface can be covered with either a monolayer and multilayer chloride film; thus, observations suggesting either type of surface film can be rationalized.

Experimental

The aluminum samples were 99.98% purity annealed foils, 100 μm thick with a typical grain size of 100 μm, manufactured for use in aluminum electrolytic capacitors (Toyo). The large grain size found in such capacitor foils is due to extensive annealing treatments after rolling, *e.g.*, for 5-6 h at 600°C.[22] The foils were pretreated for etching by open circuit immersion in 1 M NaOH at room temperature for various times, and then rinsed in deionized (DI) water. Solutions for both etching and pretreatment were prepared from reagent grade chemicals and DI water. Etching was carried out at constant applied current at 70°C, in solutions containing a mixture of 1 M HCl and 3 M H_2SO_4. Parallel experiments to identify kinetics of uniform corrosion processes were conducted in 3 M H_2SO_4. The etchant solution was circulated with a magnetic stirring bar. The counter electrode was a Pt wire fixed in place onto a glass holder containing the aluminum foil. The reference electrode (Ag/AgCl/4N KCl) was positioned behind the holder, thus away from the current path. All quoted potentials are with respect to this reference. The foil contacted the etchant solution for a standard time 10 s before application of anodic current. The current was supplied by a potentiostat-galvanostat (EG&G PAR 273), and the potential transient during etching was recorded with a high speed voltmeter (Keithley 194A) interfaced to a computer. The etched surface topography was observed with SEM (JEOL JSM-840A).

* Electrochemical Society Active Member.
z E-mail: krhebert@iastate.edu

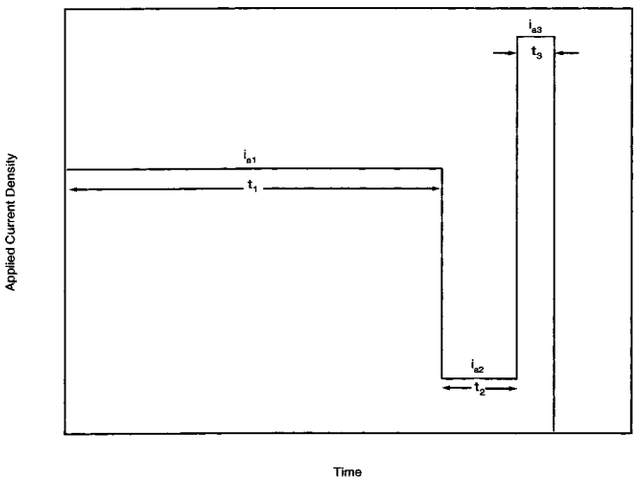

Figure 1. Schematic applied current waveform used in experiments on aluminum dissolution kinetics in etch tunnels.

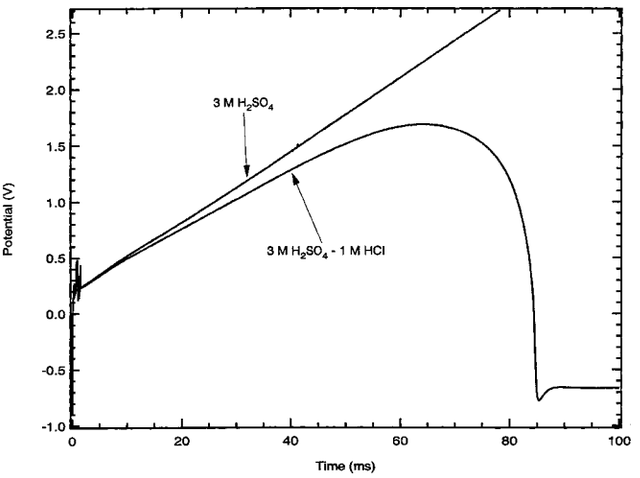

Figure 2. Potential transient during etching in a solution of 1 M HCl and 3 M H_2SO_4, for 30 s NaOH pretreatment time. Also shown is potential transient in 3 M H_2SO_4, for the same pretreatment and experimental conditions as etching experiment. Temperature 70°C, applied current density 0.2 A/cm^2.

Transient experiments were carried out to determine current/potential relationships for uniform corrosion and dissolution from etch pits. The current was kept constant for a time less than 100 ms, and then reduced rapidly through a series of steps at intervals of 0.4 ms. The accompanying potential transient was measured, and used to construct current/potential relations relevant to the pitting and uniform corrosion processes. Other experiments were conducted to measure the mean current dissolution density in etch pits. In these experiments, constant current was applied for brief periods less than 100 ms. The mean pit current density was obtained by dividing the overall pitting current by the total pit surface area from SEM. In all experiments on the kinetics of dissolution from pits, the NaOH pretreatment time was 30 s. Potentials were corrected for cell ohmic resistance, which was measured as described earlier.[13] The cell resistance for the 1 M HCl-3 M H_2SO_4 etchant solution was 0.952 Ω cm^2, and that of cell with 3 M H_2SO_4 alone was 1.04 Ω cm^2.

Measurements of dissolution kinetics in etch tunnels were carried out using a current step waveform developed previously in a study of etching in 1 M HCl.[21] That waveform is illustrated in Fig. 1, where symbols for the various current levels and step times are defined. The applied current was held constant at the initial value i_{a1} for a time t_1 of either 1 or 5 s, then reduced to i_{a2} for a time t_2 of 12 ms, and finally increased to i_{a3} for a time t_3 of 8 ms. During the period at i_{a1}, tunnels grew to a length determined by their growth velocity, which was found to be 2.1 μm/s for the present foil and etching conditions, using the applied current sawtooth wave technique.[19] The step current reduction to i_{a2} passivated a fraction $1 - (i_{a2}/i_{a1})$ of the dissolving tunnel tip surface, but did not alter the dissolution current density.[14] The step increase to i_{a3} forced a higher current through the unpassivated portion of the tunnel tip. The current density on the active portion of the tip was then $i_{d0}(i_{a3}/i_{a2})$, where i_{d0} is 6.1 A/cm^2, the equivalent current density of the 2.1 μm/s dissolution velocity. The accompanying potential transient was measured to obtain the driving force for dissolution.

Results and Discussion

Current step experiments.—Potential transients in the 1 M HCl-3 M H_2SO_4 etchant are shown in Fig. 2. After an abrupt increase in the first millisecond due to capacitive charging, the potential rose more slowly to a maximum, and then fell rapidly to a final constant potential. That final potential was identified as the repassivation potential of aluminum, and is maintained as long as the applied current is kept at the same value.[23,24] SEM images of the foil surface at times during the ''peaked'' transients in Fig. 2 show large numbers of 0.1-1 μm wide etch pits, most of which have circular outlines (Fig. 3). This circular profile is consistent with the hemispherical pit shape evident in oxide replicas of the metal surface.[18,25] No tunnels were found in these replicas. Pit number densities estimated from such images, at different etching times, are given in Table I. It is clear that pit nucleation proceeded at a high rate during the peaked transients.

Along with a potential transient during anodic etching, Fig. 2 also shows one measured in 3 M H_2SO_4, using identical pretreatment and experimental conditions. The two types of transients were nearly coincident through most of the period when the potential increased toward the maximum. No pitting, but only anodic oxide growth and uniform metal dissolution, occurred in the sulfuric acid solution.[26] Therefore, despite ongoing pit nucleation in the etchant,

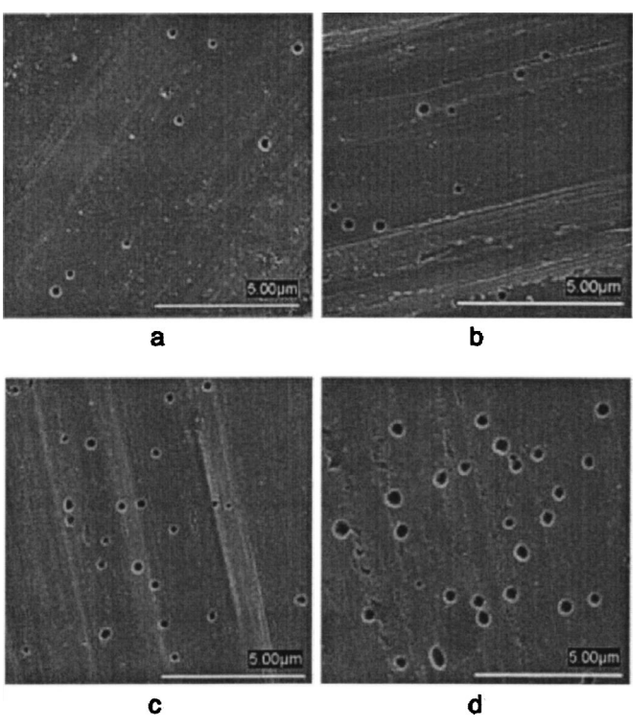

Figure 3. SEM images corresponding to various etching times during the initial increasing portion of the potential transient. Etching conditions were the same as in Fig. 2. (a) 10 ms etching time; (b) 20 ms; (c) 30 ms; (d) 55 ms.

Table I. Statistics of etch pit distributions and uniform corrosion current density.

Etching time (ms)	N_{pit}, pit number density (times 10^6 cm^{-2})	$\sigma(N_{pit})$ (times 10^6 cm^{-2})	r_{rms}, Pit radius (μm)	Square root of $\sigma(r^2)$ (μm)	Uniform corrosion current density (A/cm^2)
10	4.2	1.2	0.085	0.064	0.183
20	4.6	1.7	0.11	0.076	0.172
30	4.9	0.73	0.16	0.098	0.162
40	6.9	1.4	0.18	0.14	0.155
55	7.1	1.3	0.24	0.16	0.096

those uniform corrosion processes dominated the overall current during most of the potential rise. After the potential maximum, the decreasing potential in the etchant relative to the H_2SO_4 solution indicates that the current due to uniform corrosion is reduced, due to the increasing magnitude of the dissolution current from pits. In the following, the overall current from uniform oxidation and dissolution processes is referred to as the uniform corrosion current. Figure 2 demonstrates that the contribution of uniform corrosion must be considered in the analysis of experiments at times during the potential peak.

Experiments with step reductions of applied current were used to investigate kinetics of both uniform corrosion and metal dissolution from pits. Figure 4 shows potential transients during experiments in which sequences of four current steps were initiated at various times during the potential peak in Fig. 2. Transients for parallel experiments in 3 M H_2SO_4 are displayed in Fig. 5. All potential transients in both figures followed the same trace up to the initiation of the current step sequence, thus demonstrating the high reproducibility of these experiments. The potential at 0.4 ms after each current step was corrected for the cell ohmic drop, using the cell resistances cited in the Experimental section. These potentials and the corresponding current densities for each step sequence are shown in Fig. 6 and 7, for the experiments in 3 M H_2SO_4 and 1 M HCl-3 M H_2SO_4, respectively. It was assumed that the duration of the step sequence was small enough to neglect time-dependent changes such as oxide growth or pit enlargement. With this assumption, the current/potential data for a given step sequence represents the electrode kinetics at the initiation time of the sequence.

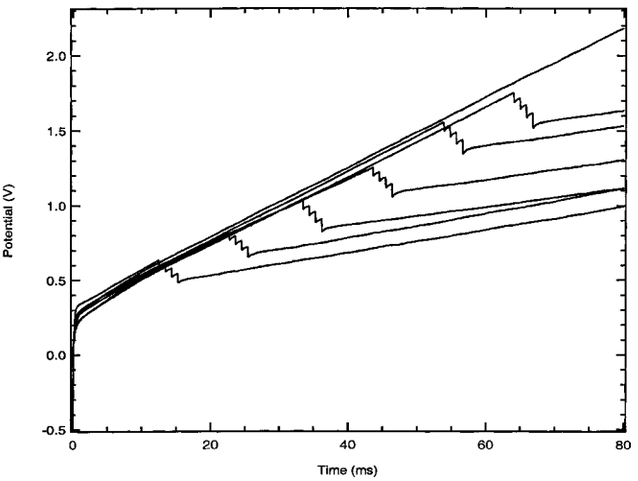

Figure 5. Potential transients in 3 M H_2SO_4, for experiments in which the applied current was reduced in a series of four steps separated by intervals of 0.4 ms. 30 s NaOH pretreatment, temperature 70°C, initial applied current density 0.2 A/cm^2.

The current/potential data in Fig. 6 and 7 were compared to calculations based on the high field rate law for ionic conduction in anodic films

$$i = i_{a0} \exp\left(\frac{B_a \phi}{\delta}\right) \quad [1]$$

This expression governs conduction in alumina films formed in acidic solutions,[26,27] and therefore was expected to model the uniform corrosion current in the present experiments. The potential drop in the oxide film, ϕ, was determined by subtracting the equilibrium potential of the Al/Al_2O_3 electrode from the ohmic-corrected potential. Enthalpy of formation data were used to extrapolate the standard potential to a value of −1.518 V *vs.* normal hydrogen electrode (NHE) at 70°C.[28] Because of the high potentials in these experiments, it was not necessary to consider additional ohmic resistance due to hydrogen gas bubbles in pits. The dashed lines in Fig. 6 and 7 represent Eq. 1, with δ obtained by fitting to the

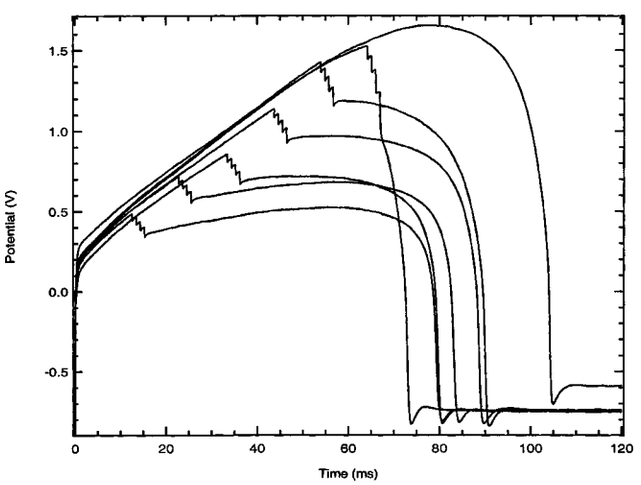

Figure 4. Potential transients in 1 M HCl-3 M H_2SO_4 etchant, for experiments in which the applied current was reduced in a series of four steps separated by intervals of 0.4 ms. 30 s NaOH pretreatment, temperature 70°C, initial applied current density 0.2 A/cm^2.

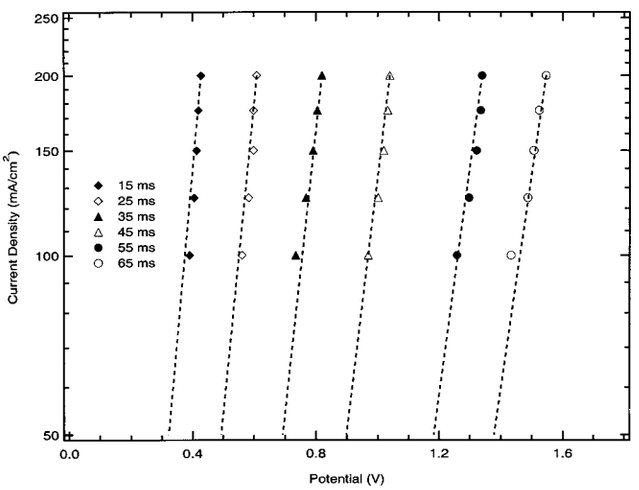

Figure 6. Applied current density *vs.* potential, from current step experiments of Fig. 5 in 3 M H_2SO_4. Potential is that measured at 0.4 ms after each current step, and was corrected for cell ohmic potential drop. Parameter is time of first current step in each sequence.

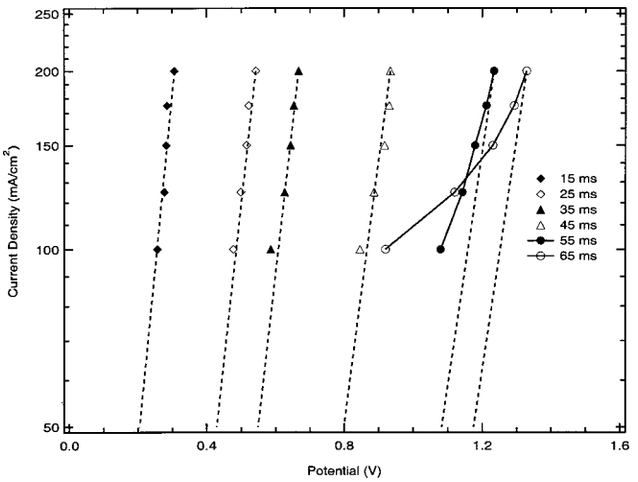

Figure 7. Applied current density *vs.* potential, from current step experiments of Fig. 4 in 3 M H_2SO_4-1 M HCl. Potential is that measured at 0.4 ms after each current step, and was corrected for cell ohmic potential drop. Parameter is time of first current step in each sequence.

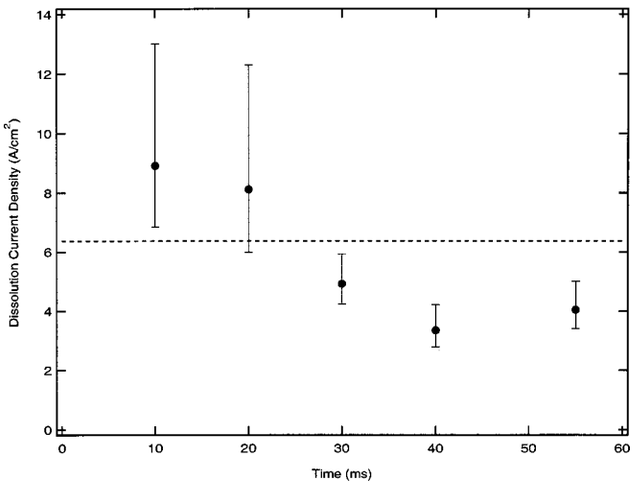

Figure 8. Average dissolution current density in pits for various etching time, obtained from pit size distributions measured using SEM. Dashed horizontal line is the average current density, 6.37 A/cm^2. Error bars represent 95% confidence intervals.

potential just prior to the step sequence. Values of the parameters i_{a0} (1.80×10^{-12} A/cm^2) and B_a (2.99 cm/MV) at 70°C were taken from measurements by Harkness and Young.[29] Figure 6 shows very good agreement between the experimental current/potential data and Eq. 1, verifying its use to model the uniform corrosion rate.

In the HCl-H_2SO_4 etchant, Fig. 7 shows that the current/potential data are well-represented by Eq. 3 up to 45 ms, but deviate significantly at 55 and 65 ms. This deviation is consistent with the etching potential transient in Fig. 2, which begins to fall below that in H_2SO_4 at 50 ms, indicating that the pitting current became appreciable at this time. Thus, at times after about 50 ms, the measured current/potential relation should be influenced by kinetics of metal dissolution from pits. The current/potential data at 65 ms are consistent with an apparent Tafel coefficient $d \ln i/dE$ of 1.6 V^{-1}. The significance of this slope with respect to the kinetic model is discussed below.

Dissolution current density from pit distribution statistics.—The mean current density for dissolution from pits was estimated by dividing the overall pitting current by the total pit area obtained from SEM images. The overall pitting current is the applied current less the uniform corrosion current, which was determined as follows: In the H_2SO_4 solution, the rate of film thickness increase obeys

$$\frac{d\delta}{dt} = \frac{\varepsilon i}{6FC_{ox}} \qquad [2]$$

where i is the applied current density, and ε is a current efficiency representing the fraction of the uniform corrosion current resulting in oxide film growth. $d\delta/dt$ may be substituted by dE/dt using Eq. 1, leading to an expression for the current efficiency for film growth

$$\varepsilon = \frac{6FC_{ox}B_a}{i \ln(i/i_{a0})} \frac{dE}{dt} \qquad [3]$$

ε calculated from Eq. 3 was found to be 0.33 ± 0.03. It was assumed that this current efficiency was also valid for the HCl-H_2SO_4 etchant, because both solutions had approximately the same pH. Thus, Eq. 3 was applied to the potential transient in the etchant, to calculate the uniform corrosion current density (i in Eq. 3) from the measured dE/dt. The overall pitting current density was then found by subtraction from the applied current density.

SEM examination of the foil surface was carried out for the times listed in Table I. As mentioned above, the pits were hemispherical in shape, so that the total pit area was $2\pi\langle r^2\rangle N_{pit}$, where the angular brackets denote the population mean. Between 40 and 120 pits were used to determine $\langle r^2\rangle$ and N_{pit} for the various etching times. The error bars in the figure are 95% calculated from the standard deviations listed in Table I. The mean pit current density is shown in Fig. 8 at the various etch times. Due to the significant uncertainty deriving from the pit distribution statistics from SEM, it cannot be distinguished whether the current density depends on time. However, the results are consistent with an average current density of approximately 6.37 A/cm^2, in agreement with the etch pit current density of 6 A/cm^2 previously estimated in HCl etchant at 70°C.[20] Also, the result agrees with dissolution current density of 6.1 A/cm^2, measured in etch tunnels formed at the same etching conditions, using a sawtooth wave superimposed on the applied current.[19] Because tunnels grow at low potentials of about −0.8 V, while measurements of the pit dissolution current density correspond to potentials of 0.5-1.6 V (Fig. 2), these results imply a roughly constant dissolution current density over a wide potential range.

The potential-insensitive dissolution current density, from tunnel growth rates and pit distribution statistics, can be compared to the results in Fig. 7 at the etch time of 65 ms. Calculation of the uniform corrosion current density at this time showed that the overall pit current furnished 97% of the applied current. Thus, the Tafel coefficient of 1.6 V^{-1} reported above represents the kinetics of metal dissolution from pits. A Tafel-like potential variation of the dissolution rate was also revealed in current pulse experiments during tunnel growth in HCl etchant.[21] These potential/dependent kinetics from current step or pulse experiments conflict with the potential-insensitive tunnel and pit growth rates. The next section reports additional current pulse experiments during tunnel growth, after which a model reconciling the various kinetic measurements is presented.

Tunnel dissolution current densities from current pulse experiments.—The potential dependence of dissolution in etch tunnels was investigated further, using the current pulse technique introduced by Tak *et al.*[21] In contrast to Tak's paper, some of the present experiments were carried out in the HCl-H_2SO_4 mixed etchant, and were extended over a considerably wider potential range. Figure 9 shows examples of two potential transients at times just after the current step from i_{a2} to i_{a3} (solid lines). In each tran-

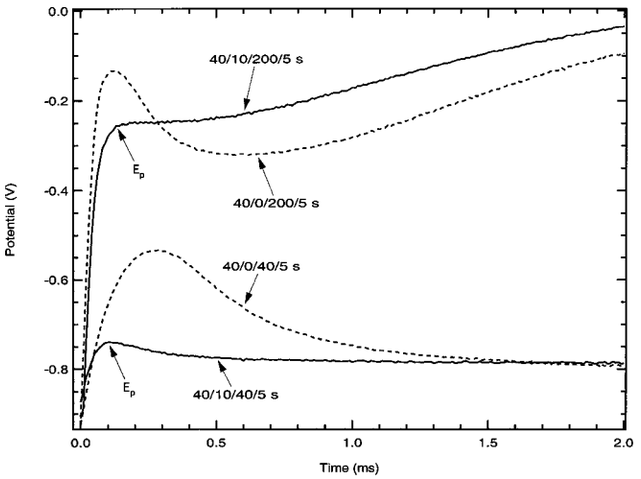

Figure 9. Examples of potential transients for current pulse experiments during etch tunnel growth. Etching temperature 70°C, etchant solution 1 M HCl-3 M H_2SO_4. Parameters in legend are $i_{a1}/i_{a2}/i_{a3}/t_1$ (see Fig. 1 for definitions), with the applied current density in mA/cm^2.

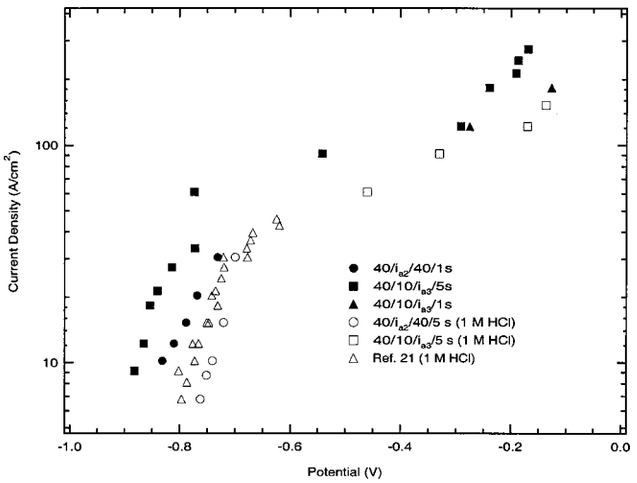

Figure 10. Metal dissolution current density from current pulse experiments, plotted *vs.* peak potential measured after current step from i_{a2} to i_{a3} (E_p in Fig. 9). Potential is corrected for cell and tunnel solution ohmic potential drops. Etchant solution 1 M HCl-3 M H_2SO_4, or 1 M HCl as indicated. Parameters in legend are $i_{a1}/i_{a2}/i_{a3}/t_1$ (see Fig. 1 for definitions), with the variable parameter denoted by a symbol, and the applied current density in mA/cm^2.

sient, the step was followed by a period of about 50 μs when capacitive charging dominated, and then a peak potential or shoulder within 0.2 ms, denoted E_p in Fig. 9. The uniform corrosion current density at this potential was estimated using Eq. 1; experiments were rejected from consideration when it exceeded 10% of the applied current density. In addition, i_{a3}, the applied current density during the anodic pulse, was found to correlate poorly with E_p, suggesting further that the current at E_p was not due to uniform corrosion. Thus, the current at E_p was supplied by metal dissolution from tunnels.

The dashed lines in Fig. 9 are potential transients from experiments with $i_{a2} = 0$, but otherwise the same current waveform parameters as the corresponding experiments with $i_{a2} > 0$. In these current interruption experiments, the potential during the anodic pulse rose to a peak value 100-300 mV higher than E_p, in a time of 0.1-0.3 ms. It was shown in Ref. 21 that the current interruption completely passivated the actively dissolving tunnel tip surface; however this surface experienced a high rate of pit initiation during the anodic pulse, resulting in recovery of the dissolution current within 0.5-1 ms. This time agrees with the decay times of the initial peaks in Fig. 9, consistent with a similar reactivation of the tip surface by pitting. Thus, potentials 100-300 mV more positive than E_p are necessary for a significant rate of pit formation on the oxide-covered part of the tunnel tip. As in Ref. 21, it is concluded that the current at E_p is supplied not by newly formed pits, but by an increased dissolution rate on the portion of the tip surface which was not passivated during t_2.

A current/potential relationship for dissolution was obtained from transients like those in Fig. 9. The current density on the unpassivated tip surface was calculated from the applied current waveform, as described in the Experimental section, and the potential driving force was obtained by correcting E_p for the cell ohmic drop. The significance of the ohmic drop inside tunnels was assessed from the potential decrease upon stepping from i_{a1} to i_{a2}.[13] It was found that tunnel length had no measurable affect on this decrease, indicating that the tunnel ohmic drop was small, likely because of the high ionic strength of the etchant. Evidence that tunnels do not contain hydrogen gas bubbles, which might contribute to the ohmic resistance, is summarized in Ref. 30. The current/potential data are shown in Fig. 10, along with those obtained in Ref. 21 using the HCl etchant. The present experiments included waveforms with high i_{a3} and low i_{a2}, yielding dissolution current densities up to 300 A/cm^2. The data in Fig. 10 are scattered, but demonstrate a trend of increasing current with potential. No dependence on etching time or current waveform parameters is evident, although the results in H_2SO_4-containing solutions appear to be displaced toward more negative potentials. A Tafel region with an exponential potential dependence is apparent at potentials higher than −0.6 V. In Ref. 21, the Tafel region was identified incorrectly to include potentials more negative than −0.6 V, as a result of the smaller potential range considered in that study.

Both the current pulse experiments in Fig. 10 and the current step experiments in Fig. 4 yield potential-dependent kinetics. In Fig. 10, the current density approaches 300 A/cm^2 at potentials lower than the range of the pit growth experiments (Fig. 2). In contrast, a much smaller and potential-insensitive dissolution current density of about 6 A/cm^2 was measured at potentials of −0.8 to −0.9 V during tunnel growth, and also at potentials higher than 1 V during pit growth. It is clear that the discrepancy in kinetic measurements is not associated with different dissolution processes in pits as opposed to tunnels, nor with the potential range of the measurements. Instead, the observation of potential-insensitive *vs.* potential-dependent dissolution rates depends on the time scale of experimental measurements. When the measurements are made less than 1 ms after current step disturbances, as in Fig. 4 and 10, the dissolution current density was found to vary with potential. However, measurements in the presence of slower potential variations, as during steady tunnel growth or in Fig. 1, yield a potential-insensitive dissolution current density of 6 A/cm^2 at 70°C. The observation of kinetics which depend on the experimental time scale is relevant to fundamental mechanism of metal dissolution, and is addressed by the kinetic model of the next section.

Kinetic model of dissolution from pits and tunnels.—The model for dissolution kinetics described here is essentially similar to the Vetter-Gorn model for metals covered with oxide films.[31,32] The Vetter-Gorn model suggests itself in the present case, because it yields potential-insensitive current densities under quasi-steady-state conditions, but potential-dependent behavior in experiments with small time scales. It is a phenomenological model which only assumes the presence of a surface metal oxide film, and independent transfer of metal and oxygen ions between the film surface and the solution. The same concepts can be applied to dissolution in pits, if it is presumed that the pit surface is covered by a multilayer or monolayer metal chloride film, with independent transfer of metal

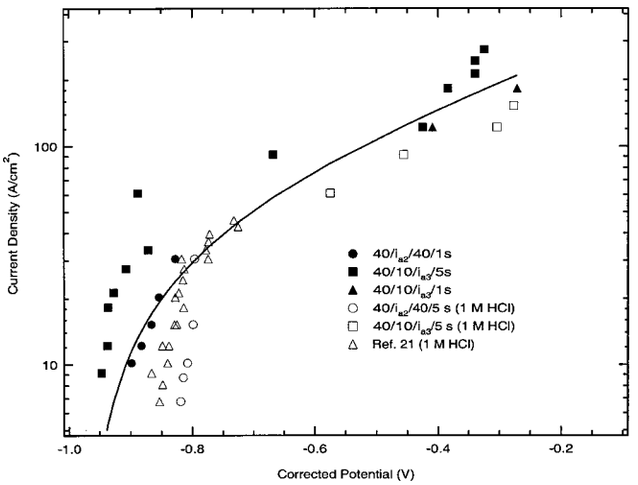

Figure 11. Dissolution current density data from Fig. 10, with potential on abscissa corrected for potential drop through chloride layer. Parameters in legend are $i_{a1}/i_{a2}/i_{a3}/t_1$ (see Fig. 1 for definitions), with the variable parameter denoted by a symbol, and the applied current density in mA/cm^2.

and chloride ions between the film surface and solution. Other authors have suggested the presence of such films on dissolving pit surfaces.[8-10] The development in this section is based on the idea that the Vetter-Gorn model can be viewed as a generic model for electrodes covered by films of corrosion products.

The corrosion product films described by the Vetter-Gorn model are distinct from precipitated salt films, which are considered by some authors to be present on dissolving surfaces in pits.[8-10] Precipitated salt films are normally thought to be in equilibrium with an adjacent saturated solution. In the Vetter-Gorn model, on the other hand, the adjacent solution is not saturated, and so ion transfer processes at the film/solution interface may not be in equilibrium. In order to focus on dissolution kinetics separately from mass transport effects, the experimental conditions of the present work were chosen so that the pit and tunnel solutions were well below saturation. The $AlCl_3$ electrolyte concentration in tunnels may be estimated from the transport model in Ref. 30, which was found to yield accurate predictions of tunnel shapes in HCl for various temperatures. For a tunnel length of 11 μm, corresponding to the maximum etch time of 5 s in Fig. 10-11, the $AlCl_3$ concentration at the tunnel tip surface is 0.8 M (Fig. 2 in Ref. 30). This value is well below the concentration of 3.1 M at saturation. The $AlCl_3$ concentration in pits should be even lower than 0.8 M, due to their smaller depth. Thus, a chloride film on the dissolving surfaces could not form by precipitation, but only by anodic oxidation of metal coupled with transfer of chloride ions from solution; these processes are the ones depicted by the Vetter-Gorn model.

The model includes mathematical descriptions for ion transport in the film as well as reactions at the film-solution interface. Ionic conduction through the film follows the rate law determined by Beck, in studies of $AlCl_3$ films on aluminum during high-rate dissolution[11,12]

$$i_f = 2i_{f0}\sinh\left(\frac{B_f\phi}{\delta}\right) \quad [5]$$

According to Beck, Eq. 5 is associated with a solid barrier-type chloride layer. The reactions at the film/solution interface are metal ion dissolution

$$Al^{+3}(f) \rightarrow Al^{+3}(aq) \quad [6]$$

and the transfer of chloride ions

$$Cl^-(f) \leftrightarrow Cl^-(aq) \quad [7]$$

It is assumed that the solution Al^{+3} concentration is low enough to neglect the reverse deposition process in Eq. 6. Thus, the charge-transfer processes in Eq. 6 and 7 are assumed to follow Tafel and Butler-Volmer kinetics, respectively, in which their rates depend on the potential drop at the film/solution interface. This potential drop, $\phi_{f/s}$, is given by $\phi_{f/s} = \phi^o_{f/s}(Cl^-) + \eta$, where $\phi^o_{f/s}(Cl^-)$ and η are the equilibrium potential drop and overpotential for Eq. 7. η', the overpotential for Al^{+3} dissolution, is then $\eta' = \phi^o_{f/s}(Cl^-) - \phi^o_{f/s}(Al^{+3}) + \eta$, where $\phi^o_{f/s}(Al^{+3})$ is the equilibrium interfacial potential drop for Eq. 6. Thus, the overpotential for Eq. 6 as well as Eq. 7 may be written in terms of η. The rate of Al^{+3} dissolution is then expressed by

$$i_C(\eta) = i_{C0}\exp(b_C\eta) \quad [8]$$

and that of chloride transfer is

$$i_L(\eta) = i_{L0}[\exp(b_L^+\eta) - \exp(-b_L^-\eta)] \quad [9]$$

The film is assumed to be composed of a constant stoichiometric proportion of Cl^- ions, so that its growth rate can be related to i_L

$$\frac{d\delta}{dt} = \frac{i_L(\eta)}{3FC_f} \quad [10]$$

The condition for current continuity between the film and interface is

$$i = i_f(\phi) = i_L(\eta) + i_C(\eta) \quad [11]$$

At the metal/film interface, metal atoms are assumed to be in equilibrium with the metal ions in the film. Thus, the measured potential E corrected for ohmic drop can be expressed as the sum of η, ϕ and the equilibrium potential at the metal/film interface

$$E = E^o_{Al/AlCl_3} + \phi + \eta \quad [12]$$

Two limiting cases of the kinetic model can be related to the present experiments. First, if the experimental time scale is large and the potential varies slowly, there is time for the film thickness to adjust to the value where Cl^- ions in the film and solution are in equilibrium. The condition $\eta = 0$ from Eq. 9 then fixes the metal dissolution current density at i_{C0} (Eq. 8). Thus, the constant current density i_{C0} is always obtained, because the Cl^- equilibrium specifies the potential driving force for metal ion dissolution. This behavior agrees with potential/insensitive dissolution rates measured during pit and tunnel growth. According to Eq. 5 and 12, the potential is then given by

$$E = E^o_{Al/AlCl_3} + \frac{\delta}{B_f}\ln\left(\frac{i_{C0}}{i_{f0}}\right) \quad [13]$$

Variations of electrode potential are accommodated by changing the quasi-steady state film thickness δ. As the potential is decreased the film becomes thinner, until at the repassivation potential it consists of one monolayer. Further potential decreases would then induce chloride desorption, and consequently passivation.[13-16]

In the limit of very small times after sudden changes of potential, the film thickness remains constant, while the potential drops η and ϕ are adjusted to maintain Eq. 11 and 12. An expression for the current density is found by writing $i = i_L(\eta) + i_C(\eta)$,

$$i = i_{L0}\{\exp[b_L^+(V - E^o_{Al/AlCl_3})] - \exp[-b_L^-(V - E^o_{Al/AlCl_3})]\} + i_{C0} \quad [14]$$

where the corrected potential $V = E - \phi$. The Tafel region in Fig. 10 is controlled by the anodic term in i_L rather than i_C, because the

current intercept at the steady-state potential is much larger than $i_{C0} = 6.1$ A/cm^2; thus, the potential dependence of i_C is neglected in Eq. 14. To calculate V, ϕ was determined from Eq. 5, with the parameters $B_f = 1.5 \times 10^{-6}$ cm/V and $i_{f0} = 0.81$ A/cm^2 obtained using results from Ref. 12. This value of i_{f0} was obtained in potential step experiments using millimeter-scale artificial pit electrodes. B_f is a theoretical estimate, representing an average of values assuming either Al^{+3} or Cl^- conduction. Tunnels grow at the repassivation potential, where the chloride layer thickness is expected to be one monolayer; hence, δ in Eq. 5 was assigned the value of 0.40 nm. Figure 11 shows the dissolution current density data from Fig. 10 plotted against the corrected potential V. Eq. 14 was fit to the entire data set, although as noted earlier separate kinetic parameters may actually apply in HCl and HCl-H_2SO_4 solutions. Although the results are scattered, Eq. 14 describes that potential dependence reasonably well. The parameter estimates obtained by fitting are $i_{L0} = 47$ A/cm^2, $b_L^+ = 2.4$ V^{-1}, $b_L^- = 1.0$ V^{-1}, and $E^o_{Al/AlCl_3} = -0.93$ V.

The interpretation of the current step experiments at 65 ms etch time in Fig. 7 is now considered. As noted earlier, nearly all the applied current at this time was supplied by pits, indicating that the current/potential trace reflects dissolution kinetics. However, unlike the current pulse experiments, the dissolution current densities in Fig. 7 are smaller than i_{C0}. Calculations with the kinetic parameters cited above showed that η was between -10 and 0 mV, while ϕ varied from 1.79 to 2.22 V. Thus, the currents in Fig. 7 are controlled by the conduction resistance of the chloride layer. According to Eq. 5, the Tafel coefficient at 65 ms should then be $B_f/\delta = \ln(i_f/i_{f0})/\phi$, where i_f and ϕ are the values prior to the current step sequence. Using $i_f = 6.1$ A/cm^2 and $\phi = E - E^o_{Al/AlCl_3} = 2.22$ V, the expected B_f/δ is then 0.91 V^{-1}, comparable to but somewhat smaller than the experimental value of 1.6 V^{-1}. This discrepancy may be due to differences between the conductivity of the chloride layer in the present 100 nm-scale etch pits *vs.* the millimeter-scale artificial pits of Ref. 11 and 12. Agreement with the experimental B_f/δ would be obtained with $i_{f0} = 0.17$ A/cm^2, compared to the assumed value of 0.81 A/cm^2. Despite this difference, the calculations based on the kinetic model, along with Beck's conduction measurements, provide a reasonable interpretation of the current step experiments, indicating that a multilayer chloride film is present in pits at high potentials.

The discussion in this section shows that the Vetter-Gorn kinetic model, when applied to the hypothesized aluminum chloride surface layer, is consistent with the measurement of a potential-dependent dissolution rate in current step or pulse experiments. The experiments with step increases of current were controlled by chloride ion transfer at the film/solution interface, while behavior after the step current decreases was determined by conduction kinetics in the chloride layer. Results of the latter experiments agree reasonably with a model for conduction in a barrier $AlCl_3$ layer.[11,12] The kinetic model also predicts the observed potential-insensitive dissolution rate in experiments where the potential changes relatively slowly. Since the measured time scale-dependent dissolution kinetics are unusual, the existence of a model which is consistent with this behavior is noteworthy.

Finally, it is emphasized that the model suggests no intrinsic difference between metal dissolution in pits and tunnels. The above calculations revealed thicker chloride layers in pits than tunnels, simply because the pit growth potentials in the particular experiments reported here (Fig. 2) were much higher than the potentials of -0.9 to -0.8 V associated with tunnel growth.

Conclusions

Kinetics of aluminum dissolution in etch pits and tunnels were investigated, during anodic etching in 1 M HCl-3 M H_2SO_4 solution at 70°C. The pit and tunnel growth current densities were found to be approximately the same, 6 A/cm^2, despite very different potentials for the experimental conditions of tunnel and pit growth (roughly -0.8 and 1 V *vs.* Ag/AgCl respectively). On the other hand, experiments with current step reductions during pitting, or with anodic current pulse modulations during tunnel dissolution, found strongly potential-dependent dissolution rates. In each of these experiments, the potential driving force for dissolution was measured within 1 ms of a current step. In the anodic current pulse experiments, the dissolution rates approached values of 300 A/cm^2 at potentials near -0.1 V, in marked contrast to the pit growth current density of about 6 A/cm^2 at higher potentials. It was concluded that potential-dependent or potential-insensitive dissolution rates are observed during either fast transient or quasi-stationary measurements, respectively.

A kinetic model for the corroding aluminum surface was developed, based on the concept of a monolayer or multilayer surface chloride layer. The model is similar to that of Vetter and Gorn for metals covered with surface oxide films.[31] Kinetic expressions were included for transfer of Al^{+3} and Cl^- ions at the film/solution interface, and ionic conduction in the film. The model predictions indicate that during quasi-stationary experiments, Cl^- equilibrium with solution is maintained, and the dissolution rate is constant. In rapid transient experiments, the film thickness is fixed and the dissolution rate is controlled by either interfacial ion transfer or conduction; a Butler-Volmer type current/potential relation is found, in agreement with experimental observations. Large anodic current densities in these experiments are associated with high rates of chloride transfer during film growth. The film thickness is expected to be one monolayer at the repassivation potential, but significantly thicker films should be present at higher potentials.

Acknowledgments

Financial support was provided by St. Jude Medical Corporation. Aluminum foils were donated by Nippon Chemi-Con Corporation.

List of Symbols

B_a, B_f	electric field coefficients for high field conduction, cm/V
b_2^+, b_2^-	empirically fit potential coefficients, V^{-1}
b_C, b_L^+, b_L^-	potential coefficients in electrochemical kinetic equations, V^{-1}
C_f, C_{ox}	concentrations of Al_2O_3 or $AlCl_3$ in surface film, mol/cm^3
E	electrode potential, V
E_0	empirically fit potential parameter, V
$E^o_{Al/AlCl_3}$	equilibrium potential at chloride film/metal interface, V
F	Faraday constant, 96,487 C/equiv
i	current density, A/cm^2
i_{a1}, i_{a2}, i_{a3}	applied current densities in Fig. 1, A/cm^2
i_a, i_C, i_L	current densities of high field conduction and interfacial reactions, A/cm^2
i_{10}, i_{20}	empirically fit pre-exponential current densities, A/cm^2
i_{a0}, i_{C0}, i_{L0}, i_{f0}	pre-exponential current densities in conduction or kinetic models, A/cm^2
N_{pit}	pit number density, cm^{-2}
r	pit depth, cm
t	time, s
t_1, t_2, t_3	times of constant current periods in Fig. 1, s
V	potential drop across film and film/solution interface, V
δ	film thickness, cm
ε	fraction of uniform corrosion current resulting in oxide formation
η	overpotential at film/solution interface, V
ϕ	potential drop in film, V

References

1. F. Hunkeler and H. Böhni, *Corrosion (Houston)*, **37**, 645 (1981).
2. F. Hunkeler and H. Böhni, in *Proceedings of the International Congress on Metallic Corrosion*, Vol. 2, p. 163, National Research Council of Canada, Ottawa (1984).
3. K. P. Wong and R. C. Alkire, *J. Electrochem. Soc.*, **137**, 3010 (1990).
4. D. W. Buzza and R. C. Alkire, *J. Electrochem. Soc.*, **142**, 1104 (1995).
5. T. R. Beck, *Electrochim. Acta*, **29**, 485 (1984).
6. G. S. Frankel, J. R. Scully, and C. V. Jahnes, *J. Electrochem. Soc.*, **143**, 1834 (1996).
7. G. S. Frankel, *Corros. Sci.*, **30**, 1203 (1990).
8. H.-H. Strehblow, in *Corrosion Mechanisms in Theory and Practice*, 2nd ed., P. Marcus, Editor, p. 243, Marcel Dekker, New York (2002).
9. T. R. Beck and R. C. Alkire, *J. Electrochem. Soc.*, **126**, 1662 (1979).
10. D. Goad, *J. Electrochem. Soc.*, **144**, 1965 (1997).
11. T. R. Beck, *Electrochim. Acta*, **30**, 725 (1985).

12. T. R. Beck and J. H. Mueller, *Electrochim. Acta*, **10**, 1327 (1988).
13. B. J. Wiersma, Y. Tak, and K. R. Hebert, *J. Electrochem. Soc.*, **138**, 371 (1991).
14. Y. Tak, E. R. Henderson, and K. R. Hebert, *J. Electrochem. Soc.*, **141**, 1446 (1994).
15. Y. Tak and K. R. Hebert, *J. Electrochem. Soc.*, **141**, 1454 (1994).
16. N. Sinha and K. R. Hebert, *J. Electrochem. Soc.*, **147**, 4111 (2000).
17. R. S. Alwitt, H. Uchi, T. R. Beck, and R. C. Alkire, *J. Electrochem. Soc.*, **131**, 13 (1984).
18. R. S. Alwitt, K. R. Hebert, and T. Makino, in *Corrosion Science: A Retrospective and Current Status-In Honor of Robert P. Frankenthal*, G. S. Frankel, J. R. Scully, H. S. Isaacs, and J. D. Sinclair, Editors, PV 2002-13, p. 314, The Electrochemical Society Proceedings Series, Pennington, NJ (2002).
19. K. Hebert and R. Alkire, *J. Electrochem. Soc.*, **135**, 2447 (1988).
20. B. J. Wiersma and K. R. Hebert, *J. Electrochem. Soc.*, **138**, 48 (1991).
21. Y. Tak, N. Sinha, and K. R. Hebert, *J. Electrochem. Soc.*, **147**, 4103 (2000).
22. Z. Ashitaka, G. E. Thompson, P. Skeldon, G. C. Wood, H. Habazaki, and K. Shimizu, *J. Electrochem. Soc.*, **147**, 132 (2000).
23. K. Hebert and R. Alkire, *J. Electrochem. Soc.*, **135**, 2146 (1988).
24. Y. Zhou and K. R. Hebert, *J. Electrochem. Soc.*, **145**, 3100 (1998).
25. N. Osawa and K. Fukuoka, *Corros. Sci.*, **42**, 585 (2000).
26. A. Despic and V. P. Parkhutik, in *Modern Aspects of Electrochemistry*, J. O'M. Bockris, R. E. White, and B. E. Conway, Editors, Vol. 20, p. 401, Kluwer Academic Publishers, New York (1989).
27. J. W. Diggle, T. C. Downie, and C. W. Goulding, *Chem. Rev. (Washington, D.C.)*, **69**, 365 (1969).
28. *NIST-JANAF Thermochemical Tables*, 4th ed., Part I, M. W. Chase, Editor, p. 156, American Institute of Physics and American Chemical Society, Woodbury, New York (1998).
29. A. C. Harkness and L. Young, *Can. J. Chem.*, **44**, 2409 (1966).
30. K. R. Hebert, *J. Electrochem. Soc.*, **148**, B236 (2001).
31. K. J. Vetter and F. Gorn, *Electrochim. Acta*, **18**, 321 (1973).
32. R. Kirchheim, *Electrochim. Acta*, **32**, 1619 (1987).